

R. M. Tooke · M. G. Blyth · P. W. Hammerton

# Oscillatory oblique stagnation-point flow towards a plane wall

Received: 17 June 2011  
© Springer-Verlag 2011

**Abstract** Two-dimensional oscillatory oblique stagnation-point flow towards a plane wall is investigated. The problem is a generalisation of the steady oblique stagnation-point flow examined by previous workers. Far from the wall, the flow is composed of an irrotational orthogonal stagnation-point flow with a time-periodic strength, a simple shear flow of constant vorticity, and a time-periodic uniform stream. An exact solution of the Navier–Stokes equations is sought for which the flow stream function depends linearly on the coordinate parallel to the wall. The problem formulation reduces to a coupled pair of partial differential equations in time and one spatial variable. The first equation describes the oscillatory orthogonal stagnation-point flow discussed by previous workers. The second equation, which couples to the first, describes the oblique component of the flow. A description of the flow velocity field, the instantaneous streamlines, and the particle paths is sought through numerical solutions of the governing equations and via asymptotic analysis.

## 1 Introduction

Flows with a stagnation-point similarity structure form a broad class of exact solutions to the Navier–Stokes equations [e.g. 1,9]. Such flow structures offer relatively simple paradigms which are useful for understanding and interpreting flow in regions of larger and more complex flow fields. In this paper, we present an exact solution describing unsteady flow at a stagnation point on a wall, in which the dividing streamline makes an oblique, time-dependent angle with the wall. Such a description may be useful in studying more complex unsteady flow phenomena, for example, the flow at the rear stagnation point which appears on a cylinder held fixed in a pulsatile stream [2]. A physical example of unsteady stagnation-point flow at a wall is provided by pulsatile blood flow through a dividing artery, or blood flow through an end-to-side anastomosis [e.g. 3].

A considerable body of research has built up on the subject of stagnation-point flows. Steady two-dimensional orthogonal stagnation-point flow towards a plane wall is described by an exact solution of the Navier–Stokes equations due to Hiemenz [e.g. 4]. An extended scenario, in which the plane wall moves at constant speed either towards or away from the stagnation-point flow, has very recently been described by Weidman and Sprague [5]. In this case, a steady flow is obtained by working in a frame of reference moving with the plate. The orthogonal stagnation-point flow solution may be generalised to encompass steady oblique stagnation-point flow, in which the dividing streamline makes contact with the wall at an acute angle [6–8]. Far from the wall, the oblique flow comprises an irrotational orthogonal stagnation-point flow, a simple shear flow with constant vorticity moving parallel to the wall, and a uniform stream directed parallel to the wall. The problem was recently revisited by Drazin and Riley [9] and Tooke and Blyth [10], who unified the previous work with reference to a free parameter which quantifies the strength of the uniform stream in the far field. In all of the aforementioned papers, an exact solution of the Navier–Stokes equations is constructed by assuming

---

R. M. Tooke · M. G. Blyth (✉) · P. W. Hammerton  
University of East Anglia, Norwich NR4 7TJ, UK  
E-mail: m.blyth@uea.ac.uk

a similarity structure in which the flow stream function depends linearly on the coordinate parallel to the wall. In this case, the problem is simply described by a set of ordinary differential equations, which must be solved numerically in general. Steady oblique stagnation-point flow impinging on a circular cylinder was studied by Weidman and Putkaradze [11, 12]. Once again, the flow is described using a coupled set of ordinary differential equations.

Grosch and Salwen [13] discussed oscillating orthogonal stagnation-point flow, in which the strength of the irrotational flow far from the wall takes the time-periodic form  $1 + \Delta \cos \omega t$ , where  $t$  is time and  $\Delta$  and  $\omega$  are positive constants representing the amplitude and frequency of the oscillations, respectively. They obtained a quasi-steady solution in the limit of low frequency, and in the high frequency limit, they demonstrated that the flow field adopts the double boundary layer structure described by Stuart [14] and Riley [15]. In this double-layered structure, a Stokes layer at the wall generates a steady-streaming motion which persists away from the wall and drives a steady-streaming layer above. Merchant and Davis [17] showed that an asymptotic solution valid in the limit of large frequency and large amplitude,  $\Delta$ , can be constructed provided that the amplitude lies below a threshold value. For a general value of the frequency of oscillation, Blyth and Hall [18] showed that when the amplitude lies above a threshold value, which depends on the oscillation frequency, the stagnation-point solution breaks down at a finite-time singularity. When the amplitude lies below the critical value, the solution is regular and time-periodic. In the case of purely oscillatory stagnation-point flow, for which the strength of the far-field flow has the form  $\Delta \cos \omega t$ , Riley and Vasantha [20] demonstrated that the solution terminates in a finite-time singularity for any value of the amplitude  $\Delta$ . They attributed the failure of the stagnation-point solution to an unsustainable steady streaming of fluid particles towards the dividing streamline from either side of the stagnation point. This results in an eruption of the boundary layers adjacent to the wall which cannot be described by the assumed similarity form. Riley [16] extended the discussion to an axisymmetric oscillatory stagnation-point flow at a plane wall and found the same singular behaviour.

Here, we discuss the related problem of oscillatory two-dimensional oblique stagnation-point flow towards a plane wall. Far from the wall, the effectively inviscid flow is composed of an irrotational orthogonal stagnation-point flow, whose strength varies periodically in time, a shear flow with constant vorticity, and a uniform stream whose strength is time-periodic. Our primary goal is to describe the flow structure as it evolves throughout one time period and to discuss how this flow structure depends on the various flow parameters. This is accomplished via numerical solutions of the governing equations and an asymptotic description of the flow field in the limit when the amplitude and frequency of the oscillatory part of the far-field orthogonal flow component are both large. In common with the studies of steady stagnation-point flow mentioned above, a viscous solution near to the wall is sought by assuming a linear dependence on the wall coordinate. The flow is described by a pair of partial differential equations depending on time and on the vertical coordinate perpendicular to the wall. The governing equation that describes the oblique flow component is coupled to the orthogonal flow and cannot be solved in isolation. In contrast, the governing equation for the orthogonal flow component is independent of the oblique flow and may be solved independently. Consequently, the asymptotic results of Merchant and Davis [17] and Blyth and Hall [18] for large amplitude and frequency may be applied directly, and only the asymptotic solution of the oblique equation needs to be determined.

In the next section, we present a formal statement of the problem. In Sect. 3, we describe the structure of the near-wall flow through numerical solutions of the governing equations. In Sect. 4, we present an asymptotic analysis for large amplitude and frequency. We conclude with a discussion of our findings in Sect. 5.

## 2 Problem statement

We consider the oscillatory two-dimensional oblique stagnation-point flow of a viscous fluid towards a plane wall situated at  $y = 0$ . The flow may be represented using a stream function,  $\psi(x, y)$ , so that the velocity components in the  $x$  and  $y$  directions, respectively, are  $u = \psi_y$  and  $v = -\psi_x$ . The rotational inviscid flow, which prevails in the limit  $y \rightarrow \infty$ , is given by

$$\psi = ka(t)xy + \frac{1}{2}\chi y^2 - \chi(v/k)^{1/2}b(t)y. \quad (2.1)$$

The first term on the right-hand side of (2.1) represents an orthogonal stagnation-point flow, of strength  $ka(t)$ , where  $k$  is a positive constant and  $a(t)$  is a dimensionless time-periodic modulational factor taken to be

$$a(t) = 1 + \Delta \cos \omega t, \quad (2.2)$$

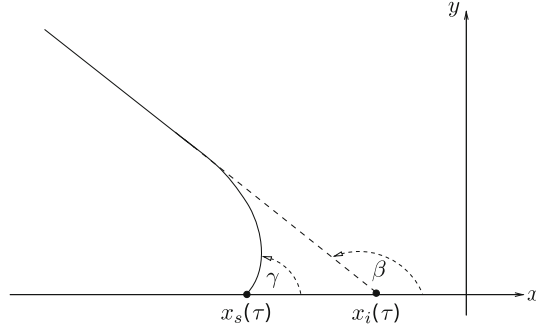


**Fig. 1** Sketch of the dividing streamline at one time instant. The *broken line* illustrates the continuation of the far-field dividing streamline to the notional wall intercept  $x_i(\tau)$  given in (2.11). The *solid line* shows how the viscous adjustment near to the wall bends the streamline towards the contact point  $x_s(\tau)$  given in (2.10)

for constant frequency  $\omega > 0$  and constant amplitude  $\Delta \geq 0$ . The second term on the right-hand side of (2.1) represents a simple shear flow, with constant vorticity  $-\chi < 0$ . The third term represents a uniform stream whose time-dependent strength is set by the dimensionless function  $b(t)$ , which we are free to choose. The complete flow (2.1) is a solution of the Euler equations provided that the vorticity  $\chi$  is constant. The solution describes an oblique stagnation-point flow whose dividing streamline, identified by  $\psi = 0$ , approaches the wall,  $y = 0$ , at an angle  $\beta$  such that  $\tan \beta = -2ka/\chi$  as is illustrated in Fig. 1.

Two characteristic far-field flow types are distinguished by the cases  $\Delta < 1$  and  $\Delta > 1$ . When  $\Delta < 1$ , the contact angle satisfies  $\beta_1 \leq \beta \leq \beta_2$ , where  $\beta_1$  and  $\beta_2$  are both obtuse angles. When  $\Delta > 1$ , the contact angle varies such that  $\beta \geq \beta_3$  and  $\beta \leq \beta_4$ , where  $\beta_3$  is an obtuse angle and  $\beta_4$  is an acute angle. This means that during the time cycle the dividing streamline sweeps down to vanish on one side of the  $x$  axis and instantaneously reappear on the other side.

Since (2.1) does not satisfy the no-slip condition at  $y = 0$ , we introduce the more general flow description

$$\psi = (vk)^{1/2}x f(\eta, t) + \chi(v/k) \int_0^\eta g(\eta', t) d\eta', \quad (2.3)$$

so that

$$u = kxf_\eta(\eta, t) + \chi(v/k)^{1/2}g(\eta, t), \quad v = -(vk)^{1/2}f(\eta, t), \quad (2.4)$$

where  $f(\eta, t)$  and  $g(\eta, t)$  are dimensionless functions which depend on the new coordinate  $\eta = (k/\nu)^{1/2}y$ . Matching the horizontal velocity component with the far-field flow (2.1), we require

$$f \sim a(t)\eta - \alpha(t) + o(1), \quad g \sim \eta - b(t) + o(1), \quad (2.5)$$

as  $\eta \rightarrow \infty$ , where  $\alpha(t)$  is a function of time to be determined, which may be interpreted as a viscous displacement of the streamlines in the far field, as will be discussed below.

Substituting (2.3) into the Navier–Stokes equations, and defining the new time variable  $\tau = \omega t$ , we obtain the following pair of partial differential equations governing  $f(\eta, \tau)$  and  $g(\eta, \tau)$ :

$$\sigma f_{\eta\tau} + f_\eta^2 - ff_{\eta\eta} = \sigma a_\tau + a^2 + f_{\eta\eta\eta}, \quad (2.6)$$

$$\sigma g_\tau + f_\eta g - fg_\eta = \alpha - ab - \sigma b_\tau + g_{\eta\eta}, \quad (2.7)$$

where the Strouhal number  $\sigma = \omega/k$ , and the time-periodic function  $a(\tau)$  is given by (2.2). At the solid boundary, the no-slip and tangential flow conditions require

$$f(0, \tau) = f_\eta(0, \tau) = 0, \quad g(0, \tau) = 0. \quad (2.8)$$

As a result of the viscous adjustment, both the angle of intercept and the point of intercept of the dividing streamline at the wall are modified from the inviscid predictions quoted above, as is illustrated in Fig. 1. It can readily be shown that the angle of intercept  $\gamma(\tau)$  varies in time and satisfies

$$\tan \gamma = 1/m, \quad m = \left(\frac{\chi}{k}\right) \frac{1}{3f_{\eta\eta}(0, \tau)} \left( (\alpha - ab - \sigma b_\tau) - (\sigma a_\tau + a^2) \frac{g_\eta(0, \tau)}{f_{\eta\eta}(0, \tau)} \right). \quad (2.9)$$

The point of intercept, which moves in time, is given by

$$x_s(\tau) = - \left(\frac{\nu}{k}\right)^{1/2} \left(\frac{\chi}{k}\right) \frac{g_\eta(0, \tau)}{f_{\eta\eta}(0, \tau)}, \quad (2.10)$$

and coincides with a point where the wall shear stress is zero. Substituting the asymptotic far-field behaviour (2.5) into (2.3), we may determine the notional wall intercept of the far-field dividing streamline, which is illustrated in Fig. 1, to be

$$x_i(\tau) = \left(\frac{\nu}{k}\right)^{1/2} \left(\frac{\chi}{k}\right) \left(\frac{b}{a} - \frac{\alpha}{2a^2}\right). \quad (2.11)$$

The first term in the final bracket represents the intercept of the inviscid dividing streamline according to (2.1), and the second term in the final bracket represents the displacement effect due to the viscous adjustment at the wall. For the special choice of the uniform stream strength  $b(\tau) = \alpha/2a$ , the far-field streamline is always directed towards the origin so that  $x_i(\tau) = 0$ .

The orthogonal flow problem, represented by (2.6), can be solved independently to obtain  $f$ . The oblique flow problem, represented by (2.7), is coupled to (2.6) and in general may be solved only once  $f$  is known. In the absence of an orthogonal flow,  $f \equiv 0$ , the solution for the oblique flow function in the presence of an oscillatory uniform stream of the form  $b(\tau) = \delta \cos(\tau + \phi)$ , for constants  $\delta$  and  $\phi$ , is given by

$$g = \eta + \delta \left[ \exp(-\sigma^{1/2} \eta / \sqrt{2}) \cos(\tau - \sigma^{1/2} \eta / \sqrt{2} + \phi) - \cos(\tau + \phi) \right], \quad (2.12)$$

which represents a simple shear flow which is superimposed onto a classical Stokes layer over a plane wall [e.g. 4, p.192]. Solutions to the uncoupled Eq. (2.6) have been discussed by a number of authors [13, 17, 18]. Merchant and Davis [17] identified an asymptotic regime for  $\sigma \gg 1$  such that  $\Delta \sim O(\sigma^{1/2})$  in which the flow decomposes into a double-layered structure comprising a viscous Stokes layer at the wall which drives a steady slip velocity which persists away from the wall. This match to the far-field flow at infinity (2.1) is effected by a second viscous layer, known as the steady-streaming layer. The asymptotic solution breaks down at a finite-time singularity when the amplitude exceeds the threshold  $\Delta_c$ . In the limit  $\sigma \rightarrow \infty$ , this is given by the asymptotic approximation

$$\Delta_c \sim 1.29\sigma^{1/2} + 0.76 + O(\sigma^{-1/2}) \quad (2.13)$$

[17, 18]. Blyth and Hall [18] showed that a similar breakdown occurs for all values of the frequency parameter  $\sigma$  and delineated the threshold curve  $\Delta_c(\sigma)$ . In general, obtaining the solution to Eqs. (2.6) and (2.7) is a numerical task. In the next section, we compute numerical solutions for moderate values of the control parameters.

### 3 Flow structure

We present a discussion of the oscillatory oblique stagnation-point flow for different parameter values based on numerical solutions of the coupled system (2.6) and (2.7) subject to the conditions (2.5) and (2.8). We integrate the governing equation for the orthogonal flow, (2.6), forward in time numerically using the Crank–Nicolson scheme described by Blyth and Hall [18]. Once  $f$  is available at each new time step, we compute the displacement  $\alpha(\tau) = \lim_{\eta \rightarrow \infty} (a\eta - f)$  and then advance (2.7) forward one time step using the Crank–Nicolson method to obtain  $g$ . The integral in the second term in (2.3) is evaluated using the trapezium rule to determine the stream function  $\psi$  at the new time step. In all of the results to be presented, the calculations were initiated from the starting profiles  $f \equiv 0$  and  $g \equiv 0$  at  $\tau = -\pi/2$ . Results are shown below over the time interval  $2\pi \leq \tau \leq 4\pi$  by which time transients have decayed.

For the first part of the discussion, we assume that there is no superimposed uniform stream, so that  $b(\tau)$  is identically zero. The particular flow structure observed during one time period depends sensitively on the amplitude  $\Delta$ . For this reason, we break the ensuing discussion into three separate subsections detailing the three characteristically different regimes. In each case, a specific discussion is presented pertaining to the typical case  $\sigma = 1$ .

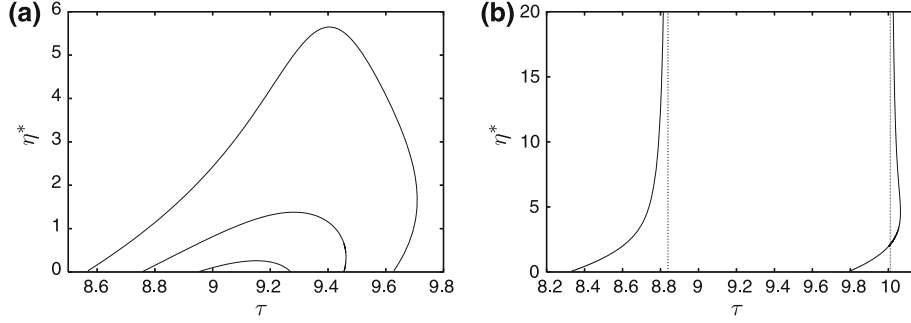


**Fig. 2** The variation of  $\eta^*$  during one time period for  $\sigma = 1.0$ : **a**  $\Delta = 0.8$  (lowermost curve),  $\Delta = 0.85$  (middle curve), and  $\Delta = 0.95$  (upper curve); **b**  $\Delta = 1.2$ ; the vertical broken lines indicate the zeros of  $a(\tau)$  at the times  $\tau = 8.84$  and  $\tau = 10.01$

- (a) Single-layered flow:  $\Delta < \Delta_1$ .

When  $\Delta < \Delta_1$ , where  $\Delta_1$  is a threshold value which depends on  $\sigma$ , the flow structure is single-layered. By this, we mean that an instantaneous streamline emanating from infinity approaches the wall, and there are no subdivisions within the flow field. Under this regime, the point of attachment  $x_s(\tau)$  roams the wall between two bounds so that the dividing streamline moves rather like a windscreen wiper swishing to and fro. For the case  $\sigma = 1$ , the threshold value  $\Delta_1 = 0.785$ .

- (b) Two-layered flow:  $\Delta_1 < \Delta < \Delta_2$ .

A different, two-layered flow pattern emerges when  $\Delta_1 < \Delta < \Delta_2$ , where  $\Delta_2$  is a second threshold value which depends on  $\sigma$ . For the case  $\sigma = 1$ , we find that  $\Delta_2 = 0.835$ . At one time during the cycle, the attachment point travels along the wall to infinity and a horizontal streamline rises up from the wall to create a streamline pattern like that shown in Fig. 3. The reason for the new flow pattern is that  $f_{\eta\eta}(0, \tau)$  becomes negative over a certain time interval during one flow period, during which time  $f$  has a zero at  $\eta = \eta^* > 0$ . This implies the presence of a horizontal streamline in the interior of the fluid (we note that in regime (a) above,  $f_{\eta\eta}(0, \tau) > 0$  throughout each flow period and so  $f$  has no zeros in  $\eta > 0$ ). By way of example, we plot  $\eta^*$  against time in Fig. 2a for the case  $\Delta = 0.8 < \Delta_2$ . The zero appears at  $\tau = 8.95$  and disappears at  $\tau = 9.27$ . Accordingly, a horizontal streamline appears at the wall at  $\tau = 8.95$ . The streamline moves upwards into the fluid before turning back and vanishing at the wall at  $\tau = 9.27$ . Referring to (2.4), we see that there is a stagnation point located on the horizontal streamline at the point

$$x^* = - \left(\frac{\nu}{k}\right)^{1/2} \left(\frac{\chi}{k}\right) \frac{g(\eta^*, \tau)}{f_\eta(\eta^*, \tau)}. \quad (3.1)$$

The instantaneous two-layered streamline pattern qualitatively resembles that shown in Fig. 3, which occurs under regime (c) to be discussed next.

- (c) Three-layered flow:  $\Delta_2 < \Delta < 1$ .

In this regime,  $f$  has one and then two positive zeros  $\eta^*$  during the period when  $f_{\eta\eta}(0, \tau)$  is negative. This is made clear by inspection of the curves for  $\Delta = 0.85$  and  $\Delta = 0.95$  (both for  $\sigma = 1$ ) in Fig. 2a. For  $\Delta = 0.95$ , the first zero appears at  $\tau = 8.56$ , and the second zero appears at  $\tau = 9.63$ . The two zeros collide and disappear at  $\tau = 9.71$ , which corresponds to the rightmost point on the relevant curve in the figure. Correspondingly, a horizontal streamline emerges from the wall and moves upwards. A short time afterwards a second horizontal streamline appears at the wall creating a three-layered structure. These two streamlines move towards each other and eventually annihilate each other whereupon the flow returns to the single-layered structure of before. The instantaneous streamline pattern during the two-layered part of the flow period is illustrated in Fig. 3. The streamline snapshot occurs at the time  $\tau = 9.13$  for the case  $\sigma = 1$  and  $\Delta = 0.85$ . The horizontal streamline can be seen at  $\eta = \eta^* = 1.2$  at this time instant. The three-layered structure is illustrated by the example shown in Fig. 4 for the case  $\sigma = 1.0$  and  $\Delta = 0.95$ . In this case, the instantaneous streamline snapshot corresponds to the time  $\tau = 9.66$ .

It is worth remarking that under this regime,  $a(\tau)$  is single-signed throughout each flow period and so the far-field flow is always moving towards the wall and spreading out towards  $x = \pm\infty$ . However, during part of one time cycle, near to the wall there are streamlines coming in from  $x = \pm\infty$  towards the origin.

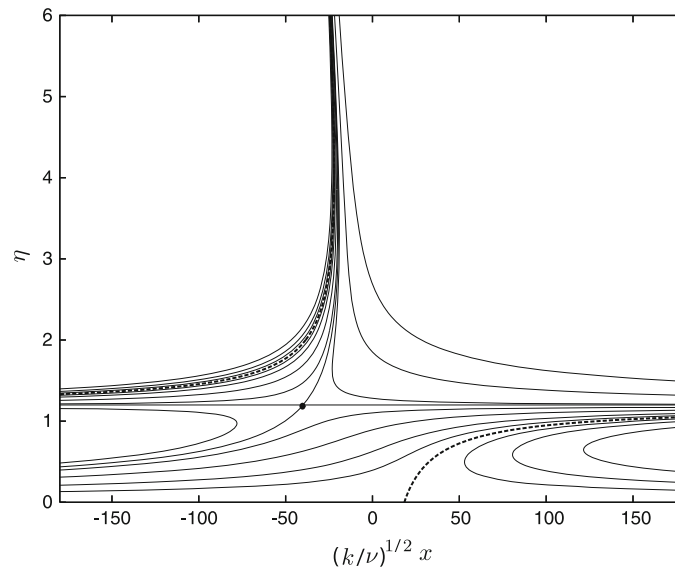


**Fig. 3** Instantaneous streamlines for the case  $\delta = 0$ ,  $\sigma = 1$ , and  $\Delta = 0.85$  shown at  $\tau = 9.13$ . At this time,  $\eta^* = 1.2$ , the stagnation point inside the fluid lies at  $x^* = -40.3$  (shown with a dot), and the attachment point lies at  $x_s = 18.4$ . The streamline  $\psi = 0$  is shown with a broken line

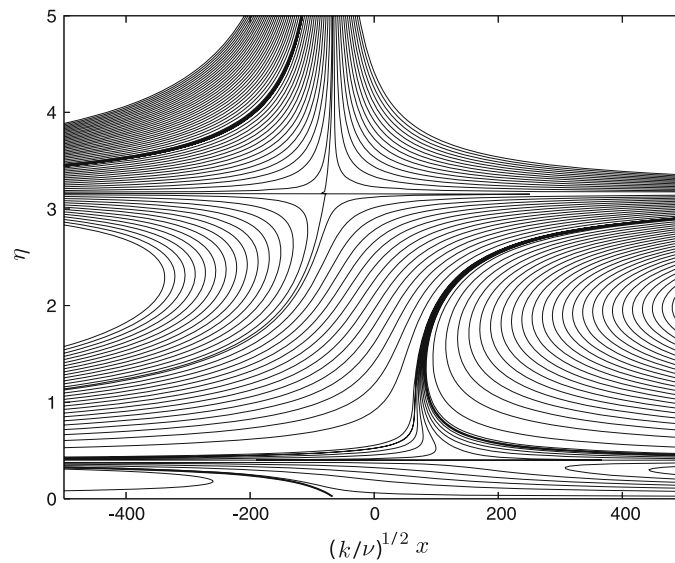


**Fig. 4** The instantaneous streamline pattern illustrating the three-layered structure at  $\tau = 9.66$  for  $\delta = 0$ ,  $\sigma = 1.0$ , and  $\Delta = 0.95$

(d) Eruption:  $\Delta \geq 1$ .

When  $\Delta \geq 1$ ,  $a(\tau)$  passes through zero during a flow period. The streamline pattern throughout one flow cycle is similar to the previous case (c) except now the horizontal streamline which emerges at the wall moves up to infinity and the flow ‘erupts’. This is evident from the trace of the zero  $\eta^*$  in Fig. 2b for the case  $\sigma = 1$ ,  $\Delta = 1.2$ . One flow period includes the following stages: first, we observe the single-layered structure with a sweeping dividing streamline; next, the double-layered structure appears as a horizontal streamline moves upwards from the wall towards infinity; then, the single-layered structure reappears; next, the double-layered structure returns—this time a second horizontal streamline emerges from infinity and descends towards the first creating a triple-layered structure. The two streamlines meet at a critical time and annihilate one another to herald the return of the single-layered flow for the remainder of the time period.

Finally, we briefly comment on the flow when  $b(\tau)$  is not zero. When  $\Delta = 0$  and  $b(\tau)$  is constant, the oblique flow is steady and has been described by previous workers [6–8]. Tooke and Blyth [10] noted that on increasing the constant value of  $b$ , the whole streamline pattern is shifted in the positive  $x$  direction. If  $\Delta = 0$  and  $b$  is not constant, the streamline pattern will change non-trivially with time. For example, although the gradient of the dividing streamline in the far field will remain constant, the angle of intercept of the dividing streamline with the wall,  $\gamma$ , which is given in (2.9), will vary in time. Calculations performed with non-zero  $b(\tau)$  may be found in Tooke [21].

#### 4 The flow at large amplitude and frequency

The pertinent asymptotic limit to study when the amplitude and frequency are both large is  $\Delta = O(\sigma^{1/2})$  [17, 18]. To study the flow in this limit, it is convenient to rescale the dependent variables in the problem by writing  $f = \Delta^{1/2} \hat{f}$ ,  $g = \Delta^{-1/2} \hat{g}$  and the independent variable by writing  $\eta = \Delta^{-1/2} \hat{\eta}$ . This permits ready comparison with the work of Merchant and Davis [17] and Blyth and Hall [18]. We introduce the inverse amplitude parameter  $\varepsilon = 1/\Delta$  and the frequency parameter  $\Omega = \varepsilon\sigma$ . In the rescaled variables, (2.6) and (2.7) become

$$\Omega \hat{f}_{\hat{\eta}\tau} + \hat{f}_{\hat{\eta}}^2 - \hat{f} \hat{f}_{\hat{\eta}\hat{\eta}} = -\Omega \sin \tau + (\varepsilon + \cos \tau)^2 + \hat{f}_{\hat{\eta}\hat{\eta}\hat{\eta}}, \quad (4.1)$$

$$\Omega \hat{g}_{\tau} + \hat{f}_{\hat{\eta}} \hat{g} - \hat{f} \hat{g}_{\hat{\eta}} = \hat{\alpha} - (\varepsilon + \cos \tau) \hat{b} - \Omega \hat{b}_{\tau} + \hat{g}_{\hat{\eta}\hat{\eta}}, \quad (4.2)$$

where  $\hat{\alpha} = \varepsilon^{1/2}\alpha$  is a function of time to be found, and  $\hat{b} = \varepsilon^{-1/2}b$  is a prescribed function of time. The matching conditions (2.5) become

$$\hat{f} \sim (\varepsilon + \cos \tau) \hat{\eta} - \hat{\alpha} + o(1), \quad \hat{g} \sim \hat{\eta} - \hat{b} + o(1). \quad (4.3)$$

At  $\hat{\eta} = 0$ , we have the no-slip and tangential flow conditions

$$\hat{f}(0, \tau) = \hat{f}_{\hat{\eta}}(0, \tau) = 0, \quad \hat{g}(0, \tau) = 0. \quad (4.4)$$

We seek an asymptotic solution to (4.1) and (4.2) in the limit of large frequency,  $\Omega \gg 1$ . Following Merchant and Davis [17] and Blyth and Hall [18], we assume that

$$\varepsilon = a_0 \Omega^{-1} + a_1 \Omega^{-2} + \dots, \quad (4.5)$$

for constants  $a_0$  and  $a_1$ . We note that (4.5) corresponds to the relation  $\Delta = a_0^{-1/2} \sigma^{1/2} + \dots$ , so that we have the relations  $\varepsilon = 1/\Delta = a_0^{1/2} \sigma^{-1/2} + \dots$  and  $\Omega = \varepsilon\sigma = a_0^{1/2} \sigma^{1/2} + \dots$ . In this limit, the mean orthogonal flow component in the far field is small in comparison with the oscillatory orthogonal flow component. For the oblique component of the flow, we will work on the assumption that the strength of the uniform stream in the far field is of the same order of magnitude as the mean orthogonal flow component in the far field. In the notation of Sect. 2, this means that  $b \sim O(1)$ . We write

$$\hat{b}(\tau) \sim [B_{00} + B_{01} \cos(\tau + \phi)] \Omega^{1/2} + [B_{10} + B_{11} \cos(\tau + \phi)] \Omega^{-1/2} + \dots, \quad (4.6)$$

where  $B_{00}$ ,  $B_{01}$ ,  $B_{10}$ ,  $B_{11}$ , and  $\phi$  are all  $O(1)$  constants. The asymptotic flow structure consists of a Stokes layer of thickness  $O(\Omega^{-1/2})$  adjacent to the wall which drives a steady-streaming layer of thickness  $O(\Omega^{1/2})$ . In the present notation, the expansions inside the Stokes layer are [17, 18]

$$\hat{f} = \Omega^{-1/2} \phi_0(\xi, \tau) + \Omega^{-3/2} \phi_1(\xi, \tau) + \dots, \quad \hat{\alpha}(\tau) = \Omega^{-1/2} A(\tau), \quad (4.7)$$

where  $\xi = \Omega^{1/2} \hat{\eta}$  is an order one variable inside the layer. For the oblique flow, in the Stokes layer, we pose the expansion

$$\hat{g} = \Omega^{1/2} \Phi_0(\xi, \tau) + \Omega^{-1/2} \Phi_1(\xi, \tau) + \dots. \quad (4.8)$$

The details of the analysis in the Stokes layer and the steady-streaming layer are given in the Appendix.

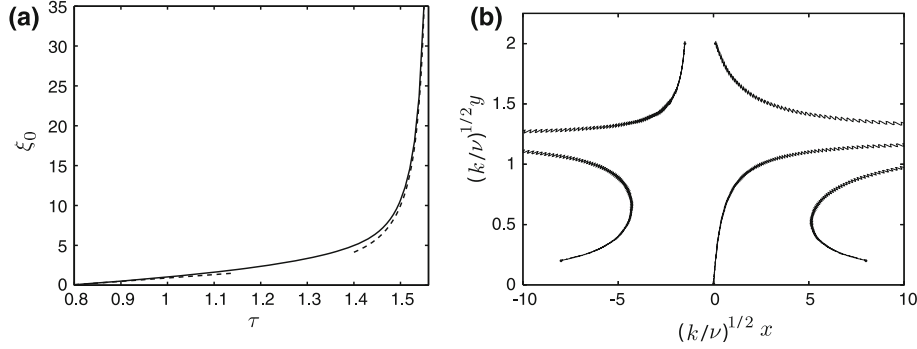


**Fig. 5** **a** The first non-trivial zero  $\xi_0$  of  $\phi_0(\xi)$  versus time  $\tau$  shown with a *solid line*. The asymptotic predictions (4.11) and (4.12) are shown with *broken lines*. **b** Particle paths for  $a_0 = 1.0$ ,  $B_{00} = 1.2$ , and  $\Omega = 100$ , plotted with  $k/\chi = 1$ . The *dots* indicate the starting points for each particle's motion

We will discuss the flow behaviour described by the asymptotic solution during the time interval  $0 \leq \tau \leq 2\pi$ . In the high frequency limit, with the scaling (4.6) for the uniform stream in the far field, the point of attachment is given by the asymptotic formula

$$x_s = \left(\frac{\nu}{k}\right)^{1/2} \left(\frac{\chi}{k}\right) a_0^{3/2} B_{01} \frac{\cos(\tau + \pi/4 + \phi)}{\cos(\tau + \pi/4)} \Omega^{-1} + O(\Omega^{-2}). \quad (4.9)$$

Evidently,  $|x_s| \rightarrow \infty$  as  $\tau \rightarrow \pi/4$  at which time we expect the double-layered structure (see scenario (c) in Sect. 3) to emerge. To scrutinise the flow around this time, we introduce the new local time variable  $\hat{T} = \tau - \frac{\pi}{4}$ , and work on the assumption that  $|\hat{T}| \ll 1$ . For small  $|\hat{T}|$ , the leading order Stokes layer solution for the orthogonal flow (A.1) becomes

$$\phi_0(\xi, \tau) \sim \left[ \frac{\xi}{\sqrt{2}} - 1 + e^{-\xi/\sqrt{2}} \cos(\xi/\sqrt{2}) \right] + \hat{T} \left[ e^{-\xi/\sqrt{2}} \sin(\xi/\sqrt{2}) - \frac{\xi}{\sqrt{2}} \right] + \dots \quad (4.10)$$

The first square-bracketed term has a simple zero at  $\xi = 0$  and is positive for  $\xi > 0$ . Balancing the leading order and first-order terms in (4.10), we find that a non-trivial zero, labelled  $\xi_0$ , appears when  $\hat{T} > 0$  and is given by

$$\xi_0 = 3\sqrt{2} \hat{T} + \dots \quad (4.11)$$

to leading order approximation for small  $\hat{T} > 0$ . The two-layered flow structure therefore emerges with the birth of the non-trivial zero,  $\xi_0$ . The horizontal streamline is located at  $\xi = \xi_0$  and moves upwards in time according to (4.11). For non-small times  $\hat{T}$ , the streamline continues to move upwards. This is evident from Fig. 5a which shows the graph of  $\xi_0$  against time over the interval  $\pi/4 < \tau < \pi/2$ . The graph was constructed by computing the zero of the leading order term in (A.1) numerically using Newton's method.

The apparently divergent behaviour of the zero,  $\xi_0$ , close to  $\tau = \frac{\pi}{2}$  seen in Fig. 5a suggests that a special investigation in the neighbourhood of this time is warranted. Accordingly, we introduce the new time variable  $T = \tau - \frac{\pi}{2}$ , with the assumption that  $|T|$  is small. By expanding the leading order solution,  $\phi_0$ , in the Stokes layer, given by (A.1), for small negative  $T$ , we find that

$$\xi_0 \sim -\frac{1}{\sqrt{2}} T^{-1}, \quad (4.12)$$

as  $T \rightarrow 0^-$ . This estimate is shown as a broken line in Fig. 5a and is almost coincident with computed zero of  $\phi_0$  near to  $\tau = \frac{\pi}{2}$ . The divergent behaviour of  $\xi_0$  in this vicinity indicates that the horizontal streamline departs the Stokes layer and moves up into the steady-streaming layer. One may continue the analysis along the preceding lines to trace the trajectory of the streamline through this layer and up into the far field. We will simply note that the horizontal streamline is found to vanish at infinity at the same instant (to within a first-order asymptotic approximation) that  $a(\tau)$  reaches zero and the dividing streamline in the far field becomes parallel with the  $x$  axis. Note that this conclusion has been reached purely by reference to the orthogonal flow

component, encapsulated by the function  $\hat{f}$ . Therefore although the function  $b(t)$  associated with the oblique flow component is taken to be  $O(1)$  here and zero in Sect. 3, comparison is still permitted between the two, and the conclusion is in accord with the numerical simulations presented in Sect. 3.

Heretofore, we have discussed the instantaneous streamline patterns encountered in the flow. However, it is difficult from these to discern the paths taken by individual fluid particles. To conclude, we present a description of the motion of a point particle placed within the flow in the high frequency, large amplitude limit. In particular, we focus attention on particle motion on the scale of the outer steady-streaming flow. The appropriate expansions for the orthogonal and the oblique flow components in the steady-streaming layer are given by (A.7) and (A.10), respectively. In the present high frequency limit, the horizontal and vertical velocity components (2.4) become

$$\begin{aligned} u &= kx \left( \frac{\Omega}{a_0} - \frac{a_1}{a_0^2} \right) [\cos \tau + \Omega^{-1} f'_0] \\ &\quad + \chi \left( \frac{\nu}{k} \right)^{1/2} a_0^{1/2} \left( 1 + \frac{a_1}{2a_0\Omega} \right) (F_1 - B_{01} \cos(\tau + \delta_1)), \\ v &= -(\nu k)^{1/2} \frac{\Omega}{a_0^{1/2}} \left( 1 - \frac{a_1}{2a_0\Omega} \right) (\zeta \cos \tau - \Omega^{-1} \cos(\tau - \pi/4) + \Omega^{-1} f_0). \end{aligned} \quad (4.13)$$

The particle paths are computed as the solution of the differential system

$$\frac{dx}{dt} = u, \quad \frac{dy}{dt} = v. \quad (4.14)$$

Recalling that  $\tau = \sigma kt$ , we find to leading order approximation  $\tau = (k\Omega^2/a_0)t$ . Inspecting the right-hand sides of (4.14), we anticipate that the particle paths will operate on the two distinct time scales  $a_0/k$  and  $\Omega^{-2}(a_0/k)$ . Accordingly, we define the new slow and fast time variables,

$$\hat{t} = \frac{k}{a_0} t \quad \text{and} \quad \hat{\tau} = \frac{k\Omega^2}{a_0} t. \quad (4.15)$$

Rewriting the second equation in (4.14) in terms of the new time scales, we obtain

$$\frac{k}{a_0\Omega^2} y_{\hat{t}} + \frac{k}{a_0} y_{\hat{\tau}} = -ky\Omega^{-1} \left( \frac{1}{a_0} - \frac{a_1}{a_0^2\Omega} \right) \cos \hat{\tau} - \Omega^{-2} \left( \frac{\nu k}{a_0} \right)^{1/2} \left( f_0 - \cos \left( \hat{\tau} - \frac{\pi}{4} \right) \right). \quad (4.16)$$

The dominant balance in (4.16) is given by  $\Omega y_{\hat{\tau}} \sim -y \cos \hat{\tau}$ . This suggests defining the new dependent variable  $Y = E^{-1} y$ , where  $E = e^{-\Omega^{-1} \sin \hat{\tau}}$ , whereupon (4.16) becomes

$$\Omega^{-2} E Y_{\hat{t}} + E Y_{\hat{\tau}} = -\Omega^{-2} \left( \frac{\nu}{k} \right)^{1/2} a_0^{1/2} \left( f_0(EY) - \cos \left( \hat{\tau} - \frac{\pi}{4} \right) \right). \quad (4.17)$$

We seek a solution in the form of the asymptotic expansion

$$Y(\hat{t}, \hat{\tau}) = Y_0(\hat{t}, \hat{\tau}) + \Omega^{-1} Y_1(\hat{t}, \hat{\tau}) + \Omega^{-2} Y_2(\hat{t}, \hat{\tau}) + \dots, \quad (4.18)$$

Substituting into (4.17), we find from the leading order and first-order equations that  $Y_0 = \tilde{Y}_0(\hat{t})$  and  $Y_1 = \tilde{Y}_1(\hat{t})$ . Integrating the second-order equation with respect to  $\hat{\tau}$ , we obtain

$$Y_2 = - \left( Y_{0\hat{t}} + \left( \frac{\nu}{k} \right)^{1/2} a_0^{1/2} f_0(Y_0) \right) \hat{\tau} + \left( \frac{\nu}{k} \right)^{1/2} a_0^{1/2} \sin \left( \hat{\tau} - \frac{\pi}{4} \right) + \tilde{Y}_2(\hat{t}), \quad (4.19)$$

where  $\tilde{Y}_2$  is a function of integration. Following the standard methodology for multiple scales, we avoid the growth of the secular term in (4.19) by demanding that

$$\tilde{Y}_{0\hat{t}} = - \left( \frac{\nu}{k} \right)^{1/2} a_0^{1/2} f_0(\tilde{Y}_0). \quad (4.20)$$

Turning to the first equation in (4.14), we introduce the new variable  $X = Ex$  and pose the expansion

$$X(\hat{t}, \hat{\tau}) = X_0(\hat{t}, \hat{\tau}) + \Omega^{-1} X_1(\hat{t}, \hat{\tau}) + \Omega^{-2} X_2(\hat{t}, \hat{\tau}) + \dots \quad (4.21)$$

Substituting the expansion, we find that  $X_0 = \tilde{X}_0(\hat{t})$  and obtain at second order

$$\tilde{X}_{0\hat{t}} = f'_0(\tilde{Y}_0) \tilde{X}_0 + \left(\frac{\nu}{k}\right)^{1/2} \left(\frac{X}{k}\right) a_0^{3/2} F_1(\tilde{Y}_0). \quad (4.22)$$

Equations (4.20) and (4.22) are solved numerically using second-order Runge–Kutta to determine the leading order particle paths. Different particle paths are found by selecting different initial conditions  $\tilde{X}_0(\hat{t} = 0)$  and  $\tilde{Y}_0(\hat{t} = 0)$ . The functions  $f_0$  and  $F_1$  on the right-hand sides of (4.20) and (4.22) are found by solving the differential systems (A.8) and (A.18) using a standard boundary value solver. Once we have found  $\tilde{X}_0(\hat{t})$  and  $\tilde{Y}_0(\hat{t})$ , we construct the particle paths by plotting the locus of the points

$$(x, y) = \left( e^{\Omega^{-1} \sin \hat{\tau}} \tilde{X}_0(\hat{t}), e^{-\Omega^{-1} \sin \hat{\tau}} \tilde{Y}_0(\hat{t}) \right), \quad (4.23)$$

for a suitably large choice of the parameter  $\Omega$ . Sample particle paths are displayed in Fig. 5b for the case  $a_0 = 1.0$ ,  $B_{00} = 1.2$  and  $\Omega = 100$ . In this limiting case, the particle paths broadly follow the streamlines associated with the steady component of the steady-streaming layer solution, with small amplitude rapid oscillations superimposed.

## 5 Discussion

We have investigated an unsteady stagnation-point flow towards a wall when the inviscid flow in the far field is composed of a time-periodic orthogonal stagnation-point flow, a shear flow with constant vorticity and a uniform stream parallel to the wall. The flow was investigated for different values of the flow parameters quantifying the strength of the oscillatory and mean orthogonal flow components, the oscillatory and mean strength of the uniform stream, and the phase difference between the uniform stream and the orthogonal flow.

In the simplest scenario, when the dimensionless amplitude of the oscillatory component of the orthogonal flow,  $\Delta$ , is sufficiently low, the flow field is characterised by a dividing streamline, which approaches the wall at an oblique angle from infinity. The dividing streamline bends as it passes through the viscous layer adjacent to the wall to make contact with the wall at a generally different angle. During the flow cycle, the point of contact sweeps along the wall, oscillating between two finite limits. The oblique angle of approach of the dividing streamline also varies in time between two definite limits.

The flow structure becomes more complex when  $\Delta$  is increased. For amplitudes  $\Delta_1 < \Delta < \Delta_2 < 1$ , where  $\Delta_1$  and  $\Delta_2$  are threshold values, the intercept of the dividing streamline with the wall moves to infinity at a critical point in the cycle, and a double-layered flow structure develops for a short time interval. A horizontal streamline emerges from the wall and migrates upwards through the fluid separating the flow into two layers. A new stagnation point emerges in the fluid interior located on the moving horizontal streamline. At the end of the short time interval, the horizontal streamline moves back down towards the wall, and the flow field recovers the previous single-layered structure. For values  $\Delta_2 < \Delta < 1$ , the upward-moving horizontal streamline is met by a second horizontal streamline descending from infinity, creating a triple-layered streamline pattern. In this case, the collision of these two streamlines heralds the return to the single-layered flow structure. When  $\Delta > 1$ , one flow period is witness to the single-layered, double-layered, and triple-layered flow structures.

When  $\Delta$  lies above a threshold value, which is dependent on the frequency of the oscillatory orthogonal flow, solutions to the governing equations are singular and terminate in a finite-time singularity. We have conducted an asymptotic analysis in the limit of large amplitude and frequency close to the threshold value. The results of the analysis corroborate the observations of the numerical simulations. For large amplitude, one time period includes two intervals during which the streamline pattern becomes multi-layered. During the first interval, a horizontal streamline appears at the wall and moves upwards to infinity. In the second interval, after the appearance of the horizontal streamline at the wall, a second horizontal streamline moves down from infinity, and the two merge.

Using a multiple scales analysis, we determined the motion of point particles within the steady-streaming layer in the large amplitude and large frequency limit. Essentially, the particle paths follow the streamlines associated with the steady component of the steady-streaming layer solution, with rapid oscillations superimposed.

## Appendix

We present the details of the asymptotic analysis for the high frequency flow discussed in Sect. 4. For reference, we note that the solution  $\phi_0$  appearing in (4.7) is given by [17]

$$\phi_0(\xi, \tau) = \xi \cos \tau - \cos(\tau - \pi/4) + e^{-\xi/\sqrt{2}} \cos(\tau - \xi/\sqrt{2} - \pi/4). \quad (\text{A.1})$$

The solution  $\phi_1$  is rather lengthy. Here, we simply note that  $\phi_{1\xi} \rightarrow -3/4$  as  $\xi \rightarrow \infty$ .

The problem for the oblique flow, given by (4.2) together with the second condition in (4.3) and the third condition in (4.4), depends on the solution to the orthogonal flow problem. In the Stokes layer, we pose the expansion (4.8). Substituting (4.6), (4.5), (4.7), and (4.8) into (4.2), we obtain at leading order,  $O(\Omega^{3/2})$ ,

$$\Phi_{0\tau} = B_{01} \sin(\tau + \phi) + \Phi_{0\xi\xi}, \quad (\text{A.2})$$

which is independent of the leading order orthogonal flow function  $\phi_0$ . The solution satisfying  $\Phi(0, \tau) = 0$  is

$$\Phi_0(\xi, \tau) = c_0 \xi + B_{01} \left[ e^{-\xi/\sqrt{2}} \cos(\tau + \phi - \xi/\sqrt{2}) - \cos(\tau + \phi) \right], \quad (\text{A.3})$$

where  $c_0$  is a constant to be determined. At first order,  $O(\Omega^{1/2})$ , we find

$$\Phi_{1\tau} + \phi_{0\xi} \Phi_0 - \phi_0 \Phi_{0\xi} = -B_{00} \cos \tau - B_{01} \cos \tau \cos(\tau + \phi) + B_{11} \sin(\tau + \phi) + \Phi_{1\xi\xi}. \quad (\text{A.4})$$

We may seek a solution in the form

$$\Phi_1 = F(\xi) + \left\{ G_1(\xi) e^{i\tau} + G_2(\xi) e^{2i\tau} + \text{c.c.} \right\}, \quad (\text{A.5})$$

where  $F$  is real,  $G_1$ , and  $G_2$  are complex, and c.c. denotes the complex conjugate. Exact solutions for  $F$ ,  $G_1$ , and  $G_2$  satisfying the boundary conditions  $F(0) = G_1(0) = G_2(0) = 0$  may be derived without difficulty, but since the resulting expressions are somewhat lengthy we will simply note that

$$\begin{aligned} \Phi_1 \sim c_1 \xi + \frac{3}{2\sqrt{2}} B_{01} \cos\left(\phi + \frac{\pi}{4}\right) + c_0 \cos\left(\tau + \frac{\pi}{4}\right) \\ - B_{00} \sin \tau - B_{11} \cos(\tau + \phi) + \text{edt}, \end{aligned} \quad (\text{A.6})$$

as  $\xi \rightarrow \infty$ , where  $c_1$  is a constant and edt stands for exponentially decaying terms. The value of  $c_1$  will be fixed through the match with the steady-streaming layer to be discussed below.

Inside the steady-streaming layer, which is of thickness  $O(\Omega^{1/2})$ , we introduce the new independent variable  $\zeta = \Omega^{-1/2} \hat{\eta}$ , where  $\zeta = O(1)$ . In this region, Merchant and Davis [17] showed that it is appropriate to write

$$\hat{f} = \Omega^{1/2} \zeta \cos \tau - \Omega^{-1/2} \cos(\tau - \pi/4) + \Omega^{-1/2} f_0(\zeta) + \Omega^{-3/2} [\psi_1(\zeta, \tau) + f_1(\zeta)] + \dots, \quad (\text{A.7})$$

where the functions  $\psi_j$ , for  $j = 1, 2, 3, \dots$ , have zero time average over a period. The leading order steady component  $f_0$  satisfies the system [see 18]

$$f_0''' + f_0 f_0'' - f_0'^2 + a_0^2 = 0, \quad (\text{A.8})$$

where a prime denotes differentiation with respect to  $\zeta$ , with  $f_0(0) = 0$ ,  $f_0'(0) = -3/4$  and  $f_0'(\infty) = a_0$ . The first-order steady component satisfies the system

$$f_1''' + f_0 f_1'' - 2f_0' f_1' + f_0'' f_1 = \frac{1}{2\sqrt{2}} f_0'' - 2a_0 a_1, \quad (\text{A.9})$$

with  $f_1(0) = 13/(4\sqrt{2})$ ,  $f_1'(0) = 0$  and  $f_1'(\infty) = a_1$ . Guided by (A.6), we expand the stream function for the oblique flow in the streaming layer by writing

$$\hat{g}(\zeta, \tau) = \Omega^{3/2} \{\Psi_0(\zeta, \tau) + F_0(\zeta)\} + \Omega^{1/2} \{\Psi_1(\zeta, \tau) + F_1(\zeta)\} + \dots. \quad (\text{A.10})$$

Substituting this expansion into the governing Eq. (4.2), it is straightforward to show that the solutions to the leading and first-order problems are

$$\Psi_0 \equiv 0, \quad \Psi_1 = (\zeta F'_0 - F_0) \sin \tau - B_{01} \cos(\tau + \phi). \quad (\text{A.11})$$

At next order,  $O(\Omega^{1/2})$ , we find

$$\begin{aligned} \Psi_{2\tau} + (\Psi_1 + F_1) \cos \tau + f'_0 F_0 - \zeta(\Psi_{1\zeta} + F'_1) \cos \tau + \cos(\tau - \pi/4) F'_0 - f_0 F'_0 \\ = -B_{00} \cos \tau - B_{01} \cos \tau \cos(\tau + \phi) + B_{11} \sin(\tau + \phi) + F''_0. \end{aligned} \quad (\text{A.12})$$

Averaging (A.12) over one time period, we find

$$F''_0 + f_0 F'_0 - f'_0 F_0 = 0. \quad (\text{A.13})$$

Matching to the Stokes layer, we require that  $F_0 \sim c_0 \zeta$  as  $\zeta \rightarrow 0$ , and matching to the far-field flow, we require that  $F_0 \rightarrow 0$  as  $\zeta \rightarrow \infty$ . The general solution to (A.13) is given by

$$F_0 = \alpha_1 f''_0(\zeta) + \alpha_2 h(\zeta), \quad h = f''_0 \int_0^\zeta [f''_0(s)]^{-2} e^{-\int_0^s f_0(r) dr} ds, \quad (\text{A.14})$$

for arbitrary constants  $\alpha_1$  and  $\alpha_2$ . Following an argument similar to that presented by Glauert [22], it can be shown that

$$h \sim \kappa_1 \zeta + \kappa_2, \quad (\text{A.15})$$

as  $\zeta \rightarrow \infty$ , where the coefficients  $\kappa_1$  and  $\kappa_2$  are constant. The constant  $\kappa_1$  may be computed by solving (A.8) numerically for a specific choice of  $a_0$ . The results of Merchant and Davis [17] and Riley and Weidman [19] indicate that there are no solutions of the orthogonal streaming problem (A.8) when  $a_0 < 0.602$ , there are two solutions when  $0.602 < a_0 < 3/4$ , and there is a unique solution when  $a_0 > 3/4$ . Taking the limit  $\zeta \rightarrow \infty$  in (A.13), we see that  $\kappa_2 = -c\kappa_1/a_0$ , where

$$c = \lim_{\zeta \rightarrow \infty} (a_0 \zeta - f_0), \quad (\text{A.16})$$

is the average value of  $A(\tau)$  over one time period. In view of this, and the facts that  $h(0) = 0$  and  $f''_0(0) \neq 0$ , we conclude that the only possibility to satisfy the matching conditions for  $F_0$  is to set

$$c_0 = 0, \quad (\text{A.17})$$

in which case  $F_0 \equiv 0$  and  $\Phi_0$  reduces to the classical Stokes layer solution represented by the time-dependent part of (2.12).

Taking the average over one time period of the equation derived at next order,  $O(\Omega^{-1/2})$ , we obtain

$$F''_1 + f_0 F'_1 - f'_0 F_1 = a_0 B_{00} - c, \quad (\text{A.18})$$

where  $c$  was defined in (A.16). The matching conditions are  $F_1(0) = 0$ ,  $F'_1(0) = c_1$  and  $F_1 \sim \zeta - B_{00}$  as  $\zeta \rightarrow \infty$ , where we recall that  $c_1$  is the constant introduced in (A.6). The solution that satisfies the boundary conditions  $F_1(0) = 0$  and the condition at infinity is

$$F_1 = a_0^{-2} (c - a_0 B_{00}) \left[ f'_0(\zeta) + \frac{3}{4 f''_0(0)} f''_0(\zeta) \right] + \kappa_1^{-1} h(\zeta). \quad (\text{A.19})$$

It is now possible to fix the as yet undetermined constant  $c_1$  by satisfying the remaining boundary condition. We find

$$c_1 = a_0^{-2} (c - a_0 B_{00}) \left[ f''_0(0) - \frac{3}{4 f''_0(0)} \left( a_0^2 - \frac{9}{16} \right) \right] + \frac{1}{\kappa_1 f''_0(0)}. \quad (\text{A.20})$$

For the sample case  $a_0 = 1$  and  $B_{00} = 1$ , we compute  $\kappa_1 = 2.257$  and  $c_1 = 0.8932$ .

---

**References**

1. Wang, C.Y.: Exact solutions of the steady-state Navier–Stokes equations. *Ann. Rev. Fluid Mech.* **23**, 159–177 (1991)
2. Qamar, A., Seda, R., Bull, J.L.: Pulsatile flow past an oscillating cylinder. *Phys. Fluids* **23**, 041903 (2011)
3. Loth, F., Fischer, P.F., Bassiouny, H.S.: Blood flow in end-to-side anastomoses. *Ann. Rev. Fluid Mech.* **40**, 367–393 (2008)
4. Batchelor, K.: *An Introduction to Fluid Dynamics*. CUP, Cambridge (1967)
5. Weidman, P.D., Sprague, M.A.: Flows induced by a plate moving normal to stagnation-point flow. *Acta Mech.* **219**, 219–229 (2011)
6. Stuart, J.T.: The viscous flow near a stagnation-point when the external flow has uniform vorticity. *J. Aero. Sci.* **26**, 124–125 (1959)
7. Tamada, K.: Two-dimensional stagnation-point flow impinging obliquely on a plane wall. *J. Phys. Soc. Jpn.* **46**, 310–311 (1979)
8. Dorrepaal, J.M.: An exact solution of the Navier–Stokes equation which describes non-orthogonal stagnation-point flow in two dimensions. *J. Fluid Mech.* **163**, 141–147 (1986)
9. Drazin, P.G., Riley, N.: *The Navier–Stokes Equations: A Classification of Flows and Exact Solutions*. CUP, Cambridge (2006)
10. Tooke, R.M., Blyth, M.G.: A note on oblique stagnation-point flow. *Phys. Fluids* **20**, 033101 (2008)
11. Weidman, P.D., Putkaradze, V.: Axisymmetric stagnation flow obliquely impinging on a circular cylinder. *Eur. J. Mech. Fluids B* **22**, 123–131 (2003)
12. Weidman, P.D., Putkaradze, V.: Erratum to “axisymmetric stagnation flow obliquely impinging on a circular cylinder”. *Eur. J. Mech. Fluids B* **24**, 788–790 (2004)
13. Grosch, C.E., Salwen, H.: Oscillating stagnation point flow. *Proc. R. Soc. Lond. A* **384**, 175–190 (1982)
14. Stuart, J.T.: Double boundary layers in oscillatory viscous flow. *J. Fluid Mech.* **24**, 673–687 (1966)
15. Riley, N.: Oscillating viscous flows. *Mathematika* **12**, 161–175 (1965)
16. Riley, N.: Unsteady flow at a stagnation point. *J. Fluid Mech.* **256**, 487–498 (1993)
17. Merchant, G., Davis, S.: Modulated stagnation-point flow and steady streaming. *J. Fluid Mech.* **198**, 543–555 (1989)
18. Blyth, M.G., Hall, P.: Oscillatory flow near a stagnation point. *SIAM J. Appl. Math.* **63**, 1604–1614 (2003)
19. Riley, N., Weidman, P.D.: Multiple solutions of the Falkner-Skan equation for flow past a stretching boundary. *SIAM J. Appl. Math.* **256**, 487–498 (1989)
20. Riley, N., Vasantha, R.: An unsteady stagnation-point flow. *Q. J. Mech. Appl. Math.* **42**, 511–521 (1989)
21. Tooke, R.M.: Stagnation-point flows. PhD thesis, University of East Anglia, Norwich (2010)
22. Glauert, M.B.: The laminar boundary layer on oscillating plates and cylinders. *J. Fluid Mech.* **1**, 97–110 (1956)